Chemical differentiation along the CepA-East outflows

C. Codella, R. Bachiller, M. Benedettini, P. Caselli, S. Viti, Valentine Wakelam

▶ **To cite this version:**

C. Codella, R. Bachiller, M. Benedettini, P. Caselli, S. Viti, et al.. Chemical differentiation along the CepA-East outflows. Monthly Notices of the Royal Astronomical Society, 2005, 361, pp.244. 10.1111/j.1365-2966.2005.09165.x . hal-00261281

HAL Id: hal-00261281
https://hal.science/hal-00261281

Submitted on 13 Apr 2021

HAL is a multi-disciplinary open access archive for the deposit and dissemination of scientific research documents, whether they are published or not. The documents may come from teaching and research institutions in France or abroad, or from public or private research centers.

L'archive ouverte pluridisciplinaire **HAL**, est destinée au dépôt et à la diffusion de documents scientifiques de niveau recherche, publiés ou non, émanant des établissements d'enseignement et de recherche français ou étrangers, des laboratoires publics ou privés.

Mon. Not. R. Astron. Soc. **361,** 244–258 (2005) doi:10.1111/j.1365-2966.2005.09165.x

Chemical differentiation along the CepA-East outflows

C. Codella,[1⋆] R. Bachiller,[2] M. Benedettini,[3,4] P. Caselli,[5] S. Viti[4] and V. Wakelam[6,7]

[1]*Istituto di Radioastronomia, INAF, Sezione di Firenze, Largo E. Fermi 5, 50125 Firenze, Italy*
[2]*Observatorio Astronómico Nacional (IGN), Apartado 1143, E-28800, Alcalá de Henares (Madrid), Spain*
[3]*Istituto di Fisica dello Spazio Interplanetario, INAF, Area di Ricerca Tor Vergata, Via Fosso del Cavaliere 100, 00133 Roma, Italy*
[4]*Department of Physics and Astronomy, University College London, Gower Street WC1E 6BT, London*
[5]*Osservatorio Astrofisico di Arcetri, INAF, Largo E. Fermi 5, 50125 Firenze, Italy*
[6]*Observatoire de Bordeaux, BP 89, 33270 Floirac, France*
[7]*The Ohio State University, Department of Physics, 174 W. 18th Ave, Columbus, OH 43210-1106, USA*

Accepted 2005 April 28. Received 2005 April 22; in original form 2005 January 14

ABSTRACT

We present the results of a multiline survey at millimetre wavelengths of the Cepheus A star-forming region. Four main flows have been identified: three pointing in the southwest, northeast and southeast directions and accelerating high-density CS clumps. The fourth outflow, revealed by high-sensitivity deuterated water (HDO) observations, is pointing towards the south and is associated with conditions particularly favourable to a chemical enrichment. At the CepA-East position the emissions due to the ambient clump and to the outflows coexist and different molecules exhibit different spectral behaviours. Some species ($C^{13}CH$, C_3H_2, CH_2CO, CH_3C_2H, $HC^{18}O^+$) exhibit relatively narrow lines at ambient velocities (ambient peak). Other molecules (CO, CS, H_2S, SiO, SO, SO_2) show extended wings tracing the whole range of the outflow velocities. Finally, OCS , H_2CS, HDO and CH_3OH are associated with wings and, indeed, show wings, and also reveal a bright high-velocity redshifted spectral peak (outflow peak) which can be used to investigate the southern outflows. At ambient velocities the gas is dense ($>10^5$ cm^{-3}) and different components at distinct temperatures coexist, ranging from the relatively low kinetic temperatures ($\leqslant$50 K) measured with H_2S, CH_3OH, H_2CS and CH_3C_2H, to definitely higher-temperature conditions, $\sim$100–200 K, obtained from the SiO, SO and SO_2 spectra. For the outflow peak we derive densities of between $\sim10^4$ and $\sim10^7$ cm^{-3} and high temperatures, $\simeq$100–200 K, indicating regions compressed and heated by shocks.

The analysis of the line profiles shows that the SiO molecule dominates at the highest velocities and at the highest excitation conditions, confirming its close association with shocks. H_2S, SO_2 and SO preferentially trace more quiescent regions than SiO, and, in particular, a lack of bright H_2S emission at the highest velocities is found. OCS and H_2CS emit at quite high velocities, where the abundances of three shock tracers such as SiO, CH_3OH and HDO are higher. These results may indicate that H_2S is not the only major sulphur carrier in the grain mantles, and that OCS and H_2CS may probably play an important role on the grains, or that alternatively they rapidly form once the mantle is evaporated after the passage of a shock. Finally, the outflow peak emission has been compared with recent time-dependent sulphur chemistry models: the results indicate that, if associated with accurate measurements of the physical conditions, the CH_3OH/H_2CS column density ratio can be used as an effective chemical clock to date the age of shocked gas.

Key words: ISM: clouds – ISM: individual: CepA – ISM: jets and outflows – ISM: molecules – radio lines: ISM.

⋆E-mail: codella@arcetri.astro.it

© 2005 RAS

Downloaded from https://academic.oup.com/mnras/article/361/1/244/1022325 by CNRS - ISTO user on 13 April 2021

1 INTRODUCTION

The mass loss from young stellar objects (YSOs) produces high-velocity flows which strike the ambient medium driving shocks. Once the temperature has increased, at least to a few thousand degrees depending on the shock type, the energy barriers between neutral molecules can be overcome and the chemistry of certain species, such as the sulphuretted species, is altered significantly (see, e.g., Pineau des Forêts et al. 1993; van Dishoeck & Blake 1998 and references therein). In addition, grains are affected by shocks, with the consequent injection of molecular and atomic species in the gas phase: again, this leads to an enhancement of the abundances of several species, including S-bearing molecules. The scenario proposed by most models is that H_2S is the main reservoir of sulphur on grain mantles: once in the gas phase, H_2S is used for a fast production of SO and SO_2 (e.g. Pineau des Forêts et al. 1993; Charnley 1997). However, the lack of H_2S features in the *ISO* spectra (Boogert et al. 2000; Gibb et al. 2000), which set upper limits on the iced H_2S abundance around protostars and the detection of OCS on grains (Palumbo, Geballe & Tielens 1997) suggest that the latter may be an important sulphur carrier in the ices. This seems supported by the observations in the envelopes of massive young stars recently performed by van der Tak et al. (2003), which indicate for OCS higher excitation temperatures than for H_2S. An alternative hypothesis is that the sulphur released from the dust mantles is mainly in atomic form (Wakelam et al. 2004). In any case, once the gas phase has been enriched by the passage of a shock, other S-bearing species such as H_2CS and HCS^+ are expected to significantly increase their abundances as a consequence of the sulphur injection. Therefore, estimates of abundance ratios such as SO_2/H_2S, H_2S/OCS and H_2CS/OCS may provide us with chemical clocks to study the evolutionary stages of molecular outflows. In fact, the use of SO_2/H_2S and H_2S/OCS ratios has already led to crude age estimates of the outflows located in CB3 (Codella & Bachiller 1999) and L1157 (Bachiller et al. 2001), encouraging further studies.

The high-temperature scenario can also be applied to hot cores around protostars, which are characterized by high temperatures ($\geqslant$100 K), high densities ($\geqslant 10^6$ cm^{-3}) and a rich molecular inventory. The SO_2/H_2S ratio has been used by Hatchell et al. (1998) for massive hot cores: the inferred ages are in agreement with the dynamical times estimated from the associated outflows. Moreover, Buckle & Fuller (2003) show that the chemical evolution of sulphuretted species is also a potential probe of time-scales in low-mass star-forming regions. In summary, the effect of high-temperature chemistry on the composition of the gas hosting the star-forming process can be used as a tool to investigate the evolution of protostars.

Physical conditions and time evolution affect the sulphur chemistry in a high-temperatures environment. For instance, recently Wakelam et al. (2004) modelled the sulphur chemistry around hot-core-like environments and found that the abundances obtained depend not only on age but also on the excitation conditions of the gas. Thus, in order to use the sulphur abundance ratios as chemical clocks, care should be taken to first constrain the gas conditions. In the case of molecular outflows, it is reasonable to expect different physical and/or chemical conditions at the different velocities and thus a study of the excitation as a function of the velocity is needed. The existing observations of sulphuretted molecules have been carried out to date in an unsystematic way, and, in particular, since the wing profiles are weak, the chemical composition of the gas at high velocity has been poorly investigated. With this in mind, we carried out line observations of S-bearing species at millimetre wavelengths towards a star-forming region with well-defined high-velocity components. Cepheus A (CepA) represents well such a target: in particular, the eastern component harbours an OB3 stellar association (Goetz et al. 1998 and references therein) driving multiple outflows (e.g. Narayanan & Walker 1996; Bergin et al. 1997). Bergin et al. (1997) have studied the chemical properties of Cepheus A, showing that a large number of molecules can be easily detected, but their observations only trace the quiescent gas, this is likely to be due to the limitation in spatial and spectral resolution, which does not allow the detection of the high-velocity wings.

In this paper, we report the results of a deep millimetre survey of molecular lines in CepA. In particular, we compare line observations of SO, HCS^+, H_2CS, OCS, H_2S and SO_2 with profiles due to standard tracers of shocked gas, high-excitation conditions and of ambient emission. The main aim is to study the variation of the abundance ratios and the excitation conditions of S-bearing species along the line profiles. We find that sulphuretted molecules may be good chemical clocks for dating molecular outflows and their driving protostellar sources.

2 OBSERVATIONS AND RESULTS

The observations were performed with the Institut de Radio-Astronomie Millimétrique (IRAM) 30-m telescope at Pico Veleta (Granada, Spain) on 2001 June, 2002 September, 2003 August and 2004 June. The observed molecular species, the transitions, their upper level energies, the Einstein *A* coefficients and rest frequencies, and some observing parameters such as the half-power beam width (HPBW) and the typical system temperature ($T_{\rm sys}$), are summarized in Table 1. The integration time (ON+OFF source) ranged from approximately 1 to $\sim$18 h, depending on the intensities of the observed lines. The main beam efficiency varies from approximately 0.8 (at 81 GHz) to 0.5 (at 262 GHz). The observations were made by position switching. The pointing was checked approximately every hour by observing nearby planets or continuum sources and it was found to be accurate to within 4 arcsec. As spectrometers, an autocorrelator (AC) split into different parts (up to six) was used to allow simultaneous observations of four different transitions. Also a 1-MHz filter bank, split into four parts of 256 channels, was simultaneously used. The velocity resolutions provided by both backends, AC and 1 MHz, are shown in Table 1. When considered convenient, the AC spectra were smoothed to a lower-velocity resolution (up to $\sim$1 km s^{-1}). The spectra were calibrated with the standard chopper wheel method and are reported here in units of main-beam brightness temperature ($T_{\rm MB}$).

The multiline molecular survey has been performed towards CepA-East and, in particular, at the coordinates of the HW2 object, which is one of the YSOs thought to drive the molecular outflows: $\alpha_{2000} = 22^{\rm h}\,56^{\rm m}\,17\overset{\rm s}{.}9$, $\delta_{2000} = +62^\circ\,01'\,49\overset{''}{.}7$. In addition, we present maps of CepA-East in CS, a well-known tracer of high-density clumps, and in HDO, which traces hot gas chemistry and shocked material (e.g. van Dishoeck & Blake 1998). In particular, the heavy water emission will be used here as an alternative to H_2O, where the observations are prevented from the ground due to very strong atmospheric absorption. Water is expected to be one of the most important coolants in non-dissociative shocks (e.g. Kaufman & Neufeld 1996), since its gas-phase abundance is considerably enhanced both via high-temperature (greater than 200–300 K) reactions and by sputtering. Given the characteristics of CepA-East, it will thus be possible to examine in detail how the dense medium is affected by the occurrence of YSOs.

Table 1 reports the selected transitions and their flux $F_{\rm int}$(K km s^{-1}) integrated along the whole profile: all but $H_2{}^{34}S(2_{20}$–$2_{11})$

Downloaded from https://academic.oup.com/mnras/article/361/1/244/1022325 by CNRS - ISTO user on 13 April 2021

Table 1. List of molecular species, transitions and observing parameters.

Transition	ν_0 (MHz)	E_u (K)	A_{ul} (s^{-1})	F_{int} (K km s^{-1})	HPBW (arcsec)	T_{sys} (K)	dv(AC) (km s^{-1})	dv(1 MHz) (km s^{-1})
Selected transitions								
HDO($J_{K\_K+} = 1_{10}$–1_{11})	80 578.30	47	1.3×10^{-6}	0.58(0.05)	31	150	0.15	3.72
OCS($J = 7$–6)	85 139.12	16	1.7×10^{-6}	0.36(0.02)	29	110	0.14	–
HCS^+($J = 2$–1)	85 347.88	6	1.1×10^{-5}	0.38(0.04)	29	110	0.14	3.51
CH_3C_2H($J_K = 5_K$–4_K)	85 457.30[a]	12[a]	2.0×10^{-6}[a]	3.11(0.13)[b]	29	150	0.27	3.51
$C^{34}S$($J = 2$–1)	96 412.98	7	1.6×10^{-5}	2.16(0.18)	26	220	0.24	3.11
CS($J = 2$–1)	97 980.97	7	1.7×10^{-5}	28.03(0.14)	25	180	0.24	3.06
SO($J_K = 3_2$–2_1)	99 299.88	4	1.1×10^{-5}	14.42(0.03)	24	150	0.24	3.02
H_2CS($J_{K\_K+} = 3_{13}$–2_{12})	101 477.75	23	1.3×10^{-5}	1.01(0.03)	24	187	0.12	2.95
$^{34}SO_2$($J_{K\_K+} = 3_{13}$–2_{02})	102 031.91	8	9.5×10^{-6}	0.11(0.01)	24	130	0.11	2.94
CH_3C_2H($J_K = 6_K$–5_K)	102 547.98[a]	17[a]	3.4×10^{-6}[a]	4.16(0.14)[b]	24	200	0.23	2.90
SO($J_K = 4_3$–3_2)	138 178.64	9	3.1×10^{-5}	22.76(0.19)	17	370	0.17	2.17
CH_3OH($J_K = 3_K$–2_K)	145 103.23[a]	14[a]	1.2×10^{-5}[a]	5.64(0.15)[a]	17	280	0.08	2.07
$H_2{}^{34}S$($J_{K\_K+} = 1_{10}$–1_{01})	167 910.52	28	2.6×10^{-5}	1.11(0.23)	14	480	0.07	1.79
H_2CS($J_{K\_K+} = 6_{16}$–5_{15})	202 923.55	47	1.2×10^{-4}	2.15(0.08)	12	460	0.06	1.48
CH_3C_2H($J_K = 12_K$–11_K)	205 080.73[a]	64[a]	2.8×10^{-5}[a]	6.71(0.36)[b]	12	600	0.11	1.46
HCS^+($J = 5$–4)	213 360.64	31	2.0×10^{-4}	0.59(0.08)	12	330	0.04	1.41
$H_2{}^{34}S$($J_{K\_K+} = 2_{20}$–2_{11})	213 376.92	84	1.7×10^{-5}	$\leqslant$0.07[c]	12	330	0.04	1.41
SiO($J = 5$–4)	217 104.94	31	5.2×10^{-4}	8.71(0.24)	11	450	0.43	1.38
$C^{18}O$($J = 2$–1)	219 560.33	16	6.2×10^{-7}	47.94(0.25)	11	580	0.43	1.36
SO($J_K = 6_5$–5_4)	219 949.39	24	1.3×10^{-4}	40.74(0.30)	11	580	0.11	1.36
CO($J = 2$–1)	230 537.98	17	6.9×10^{-7}	–[d]	10	1100	0.10	1.30
$C^{34}S$($J = 5$–4)	241 016.17	34	2.8×10^{-4}	1.75(0.40)	10	990	0.10	1.24
HDO($J_{K\_K+} = 2_{11}$–2_{12})	241 561.53	95	1.2×10^{-5}	3.42(0.19)	10	68	0.05	1.24
CH_3OH($J_K = 5_K$–4_K)	241 791.44[a]	35[a]	5.8×10^{-5}[a]	8.32(0.07)[a]	10	678	0.05	1.24
H_2CS($J_{K\_K+} = 7_{16}$–6_{15})	244 047.75	60	2.1×10^{-4}	1.36(0.06)	10	890	0.05	1.23
CS($J = 5$–4)	244 935.61	34	3.0×10^{-4}	47.33(0.53)	10	1100	0.10	1.22
SO($J_K = 7_6$–6_5)	261 843.72	35	2.2×10^{-4}	52.30(0.58)	9	1300	0.09	1.15
Serendipity detections								
$HC^{18}O^+$($J = 1$–0)	85 162.21	4	3.6×10^{-5}	0.65(0.02)	29	110	0.14	–
$C^{13}CH$($J_{K\_K+} = 1_{11}$–0_{11})	85 307.69	4	1.3×10^{-6}	0.18(0.03)	29	110	–	3.51
C_3H_2($J_{K\_K+} = 2_{12}$–1_{01})	85 338.91	6	2.3×10^{-5}	1.18(0.05)	29	110	0.14	3.51
CH_2CO($J_{K\_K+} = 5_{14}$–4_{13})	101 981.43	23	1.1×10^{-5}	0.14(0.01)	24	130	0.11	2.94
CH_3OH($J_K = 10_{-2}$–10_1 E)	102 122.70	154	1.7×10^{-7}	0.08(0.01)	24	130	–	2.94
CH_3OH($J_K = 9_1$–9_0 E)	167 931.13	126	2.3×10^{-5}	2.33(0.25)	14	480	0.07	1.79
CH_3OH($J_K = 13_6$–14_5 E)	213 377.52	390	1.1×10^{-5}	0.43(0.03)	12	330	0.04	1.41
CH_3OH($J_K = 1_1$–0_0 E)	213 427.12	13	3.4×10^{-5}	2.20(0.06)	12	330	0.04	1.41
$^{34}SO_2$($J_{K\_K+} = 16_{115}$–15_{214})	241 509.05	131	8.3×10^{-5}	0.78(0.14)	10	670	–	1.24
HNCO($J_{K\_K+} = 11_{011}$–10_{010})	241 774.09	58	2.0×10^{-4}	2.81(0.20)	10	678	0.05	1.24
$^{34}SO_2$($J_{K\_K+} = 18_{117}$–18_{018})	243 935.88	163	7.0×10^{-5}	0.61(0.73)	10	890	–	1.23

[a]For CH_3OH, it refers to the J_0–J–1_0 A^+ line, while for CH_3C_2H it refers to the $K = 0$ component. [b]For CH_3C_2H the integrated flux refers to the $K = 0$, 1 pattern. [c]It refers to the 3σ noise level. [d]The CO(2–1) observations have been performed in wobbler mode losing the information at ambient velocities in order to investigate the high-velocity wings.

have been detected. The maps of CepA in $H_2S(1_{10}$–1_{01}, 2_{20}–$2_{11})$ and $SO_2(3_{13}$–2_{02}, 5_{24}–4_{13}, 16_{214}–$15_{313})$ had already been reported in a previous paper (Codella et al. 2003). The results indicate the occurrence of a rich chemistry associated with CepA-East, confirming the findings of Bergin et al. (1997). The gas surrounding this region is particularly rich in S-bearing molecules (SO, H_2S, SO_2, H_2CS, HCS^+, OCS). Also line spectra due to tracers of the high-density clumps hosting the YSOs (CS, $C^{18}O$ and CH_3C_2H) as well as tracers of hot and/or shocked material (SiO, HDO, CH_3OH) have been obtained. Moreover, the use of large bandwidths allowed us to serendipitously detect a number of other emission lines due to $HC^{18}O^+$, C_3H_2, $C^{13}CH$, CH_2CO, CH_3OH and HNCO, as shown in the lower part of Table 1. Table 2 reports the lines which have not been identified, listing the observed peak frequency, the spectral resolution, the peak temperature and the full width at half-maximum (FWHM) linewidth.

Table 2. Unidentified detections observed towards CepA-East.

Obs. frequency (MHz)	dv (MHz)	T_{MB} (mK)	FWHM (km s^{-1})
U–102 062.23(0.15)	0.31	15(3)	7.8(2.1)
U–202 811.00(0.19)	1.00	96(20)	5.3(0.9)
U–213 303.65(0.14)	1.00	101(12)	8.4(1.6)
U–216 758.40(0.47)	1.00	80(19)	9.5(1.8)

Downloaded from https://academic.oup.com/mnras/article/361/1/244/1022325 by CNRS - ISTO user on 13 April 2021

Table 1 shows that the lines detected are associated with a wide range of excitation, from a few to hundreds of K. In particular, the detection of emission due to transitions above 100 K clearly suggests the presence of high-temperature conditions, which could be associated with the presence of a hot core and/or the occurrence of shocked material and consequently requires the analysis of the maps and of the line profiles.

3 A VIEW OF CEPA-EAST: DENSE CLUMPS AND OUTFLOWS

3.1 Ambient emission

We produced relatively small CS maps of CepA-East in order to carefully study the distribution of the ambient clumps. In particular, we focused our attention on the regions where the two strings of the Very Large Array (VLA) continuum sources associated with shocks (Garay et al. 1996) and the H_2S and SO_2 clumps (Codella et al. 2003) are located. Fig. 1 shows the maps of the integrated emission

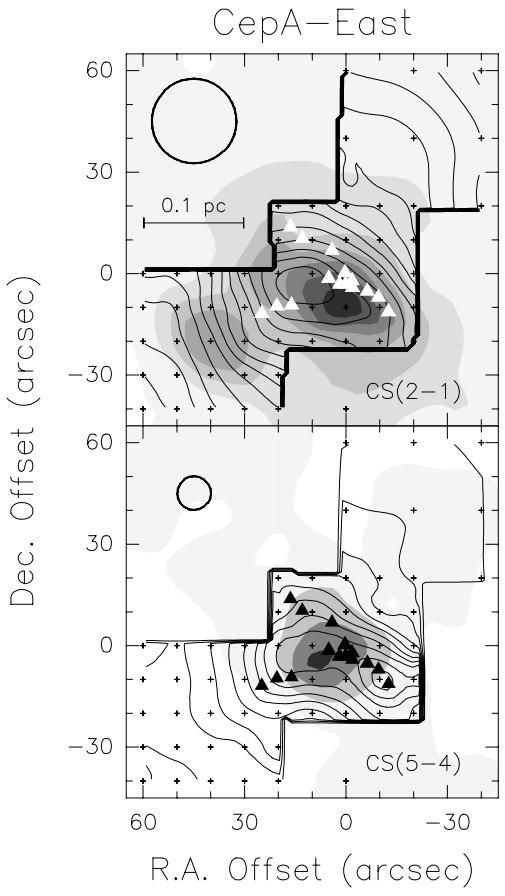

Figure 1. Contour maps of the integrated CS $J = 2$–1 (upper panel) and $J = 5$–4 (lower panel) integrated emission towards CepA-East. The maps are overlaid with the grey-scale images reproducing the integrated emission of $H_2{}^{32}S(1_{10}–1_{01})$ (upper panel) and $^{32}SO_2(3_{13}–2_{02})$ (lower panel), reported by Codella et al. (2003) in their fig. 1. The empty circles show the IRAM beam (HPBW), while the small crosses mark the observed positions. The triangles denote the VLA 2-cm continuum components which trace in the eastern region two strings of sources arising in shocks (Garay et al. 1996). The velocity integration interval is -30, $+10$ km s^{-1}. The contours range from 1.0 to 31.0 K km s^{-1} (upper panel) and from 3.0 to 57.0 K km s^{-1} (lower panel). The first contours and the steps correspond to $\sim$3- and 6σ, respectively (where σ is the rms of the map).

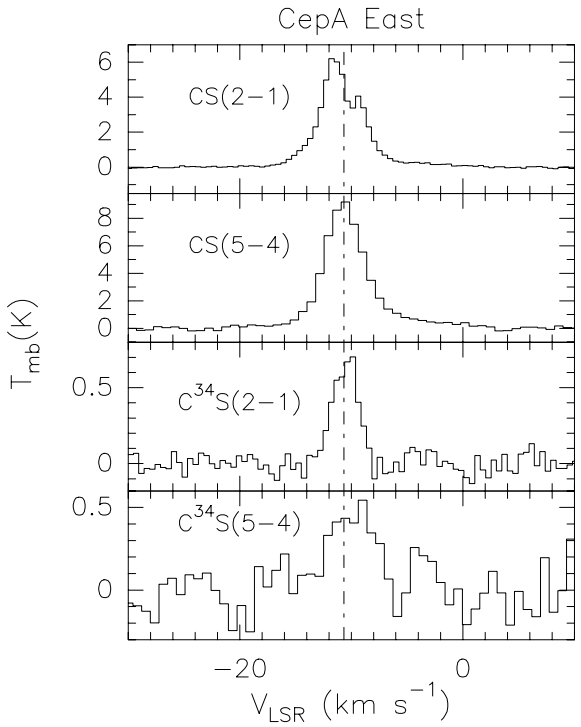

Figure 2. CS and $C^{34}S$ line profiles observed towards CepA-East: transitions are reported. The dashed line stands for the ambient LSR velocity (-10.65 km s^{-1}), according to the CS $J = 5$–4 and $C^{18}O$ $J = 2$–1 measurement (see the text).

due to CS $J = 2$–1 (upper panel) and $J = 5$–4 (lower panel) and compare such distributions with those of H_2S $J_{K-K+} = 1_{10}–1_{01}$ (upper panel) and SO_2 $J_{K-K+} = 3_{13}–2_{02}$ (lower panel), reported in grey-scale. The triangles denote the VLA objects. It is possible to note that the two CS maps peak at different positions, probably due to the self-absorption of the 2–1 line (see the self-reversed profile in Fig. 2). Also the H_2S and SO_2 emissions show a different distribution with respect to CS, indicating that such molecules are not simply reproducing the same gas distribution and are able to trace different gases associated with different physical and/or chemical conditions.

Fig. 2 reports the CS (upper panels) and $C^{34}S$ (lower panels) spectra due to the $J = 2$–1 and 5–4 transitions. Although the CS(5–4) line shows the occurrence of wings which modify the Gaussian profile at $\sim$15 per cent of the line peak, such emission can be used to define the characteristics of the ambient emission: the local standard of rest (LSR) velocity is -10.65 km s^{-1} (dashed line in Fig. 2), while the FWHM is 3.8 km s^{-1}. The comparison between these CS spectra confirms what was found in the recent paper by Bottinelli & Williams (2004) which clearly indicates that the CS(2–1) profile is affected by self-absorption, whereas CS(5–4) and the two transitions of $C^{34}S$, due to higher excitation and/or smaller abundance, are definitely optically thinner and thus well centred at the LSR ambient velocity. Moreover, as also reported by Bottinelli & Williams (2004), the CS(2–1) line shows a blueshifted peak brighter than the redshifted one, suggesting that infall motions can play an important role in the dynamics of the material traced by CS.

Fig. 3 compares the $H_2{}^{34}S(1_{10}–1_{01})$ and the $^{34}SO_2(3_{13}–2_{02})$ spectra (dotted lines, also see Fig. 1) with the profiles of the main isotopomers (continuous lines), reported in a previous paper (Codella et al. 2003). Note that the $SO_2(3_{13}–2_{02})$ profile is blended with the $16_{214}–15_{313}$ line. The comparison between the H_2S spectra indicates that the double-peak $H_2{}^{32}S$ pattern is caused by self-absorption, with

Downloaded from https://academic.oup.com/mnras/article/361/1/244/1022325 by CNRS - ISTO user on 13 April 2021

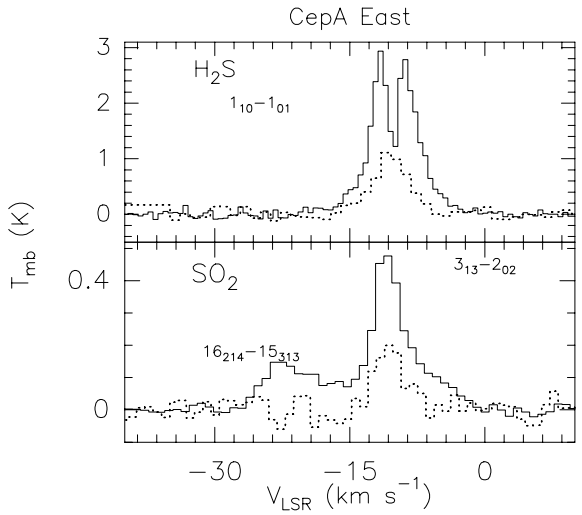

Figure 3. CepA-East: comparison between the same line transitions of different isotopomers. The solid lines are for the $H_2{}^{32}S(1_{10}–1_{01})$ and $^{32}SO_2(3_{13}–2_{02})$ profiles reported by Codella et al. (2003). The dotted lines show the corresponding $H_2{}^{34}S$ and $^{34}SO_2$ spectra, rescaled to be comparable with the ^{32}S-lines. Note that only for $^{32}SO_2$ is the $3_{13}–2_{02}$ line blended with the $16_{214}–15_{313}$ emission.

the $H_2{}^{34}S$ line peaking at the LSR velocity, where $H_2{}^{32}S$ shows the relative minimum. On the other hand, Fig. 3 confirms that the detected SO_2 lines do not present self-absorption effects and they peak at the ambient velocity.

3.2 Kinematics

Fig. 1 shows an elongated structure oriented in the NE–SW direction in the CS(5–4) line, which is not affected by self-absorption and it has been observed with an angular resolution of 10 arcsec. To further study this distribution, a CS(5–4) channel map is reported in Fig. 4. Focusing the attention on the emission at velocities close to the ambient one, which corresponds to −10.7 with a FWHM of 1.8 km s^{-1}, we note that the elongated structure is due to the presence of two clumps centred, respectively, at the (+20, 0 arcsec) and (−10, −10 arcsec) offset map positions and with a beam deconvolved size of ∼15 arcsec (0.05 pc at a distance of 725 pc, Sargent 1977) at slightly different velocities. This picture resembles the distribution of another high-density tracers such as N_2H^+ (Bergin et al. 1997): the two clumps could indicate star-forming sites or could point to gas components accelerated by the interaction with the mass loss processes indicated by the NE–SW VLA string. The latter case seems to be more likely since the clumps are symmetrically located with respect to the positions of the driving YSOs (the HW2 object is located at the centre of the map) and lie along the direction corresponding to the main axis of an extremely high-velocity outflow ($v - v_{\rm LSR} \geqslant 20$ km s^{-1}; e.g. Narayanan & Walker 1996).

On the other hand, from Fig. 4 it is possible to see (i) redshifted (up to −2 km s^{-1}) and blueshifted (up to −15 km s^{-1}) emission associated with the SW jet and (ii) a blueshifted clump located at the end of the SE VLA chain as clearly reported in the −15 km s^{-1} panel. The latter clump is also seen in H_2S at high velocities (see fig. 4 of Codella et al. 2003) and visible in Fig. 1 (upper panel) at (+40, −20 arcsec), confirming that at this position we are tracing high-density material associated with outflow motions. In conclusion, the CS emission traces two outflow directions, the SW and SE ones, associated with two strings of shocked sources.

Fig. 5 shows the contour maps of the $J_{K_-K_+} = 1_{10}–1_{11}$ and $2_{11}–2_{12}$ integrated HDO emission towards CepA-East. In particular, considering the CS results, the southern region has also been mapped to look for signposts of outflow motions. The $1_{10}–1_{11}$ emission clearly

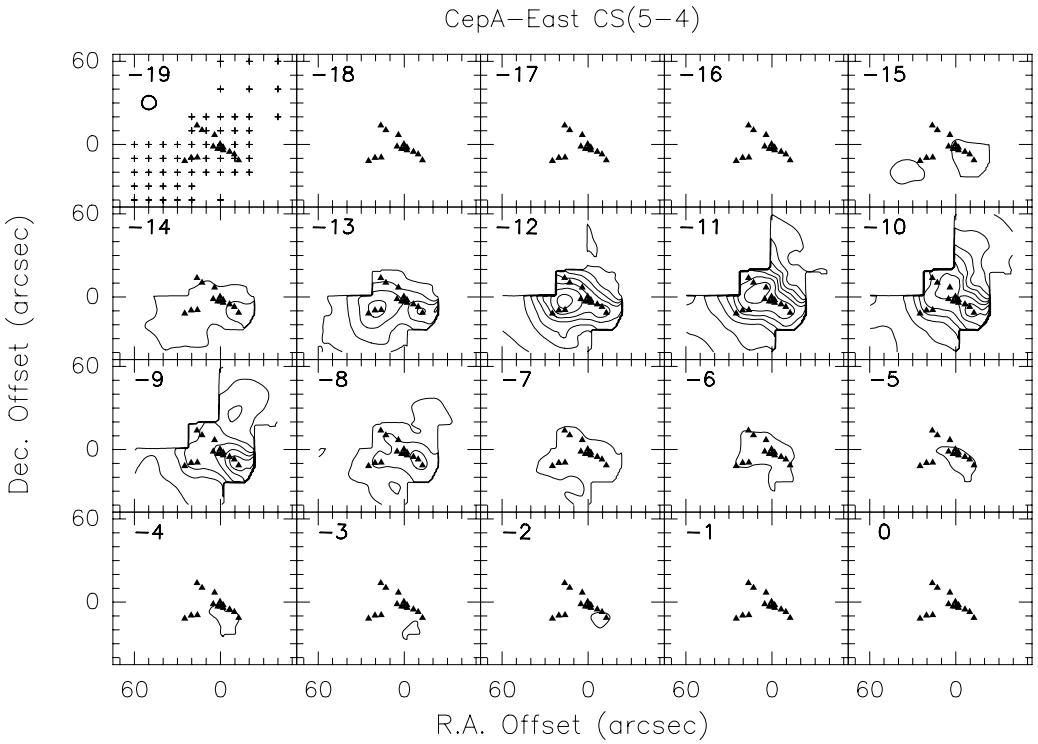

Figure 4. Channel map of the CS $J = 5–4$ emission towards CepA-East. Each panel shows the emission integrated over a velocity interval of 1 km s^{-1} centred at the value given in the left-hand corner. Symbols are drawn as in Fig. 1. The ambient velocity emission is −10.7 km s^{-1} according to CS $J = 5–4$ and $C^{18}O$ $J = 2–1$ measurements (see Section 3.2). The contours range from 0.75 (∼ 5σ) to 9.75 K km s^{-1} in steps of 1.50 K km s^{-1}.

Downloaded from https://academic.oup.com/mnras/article/361/1/244/1022325 by CNRS - ISTO user on 13 April 2021

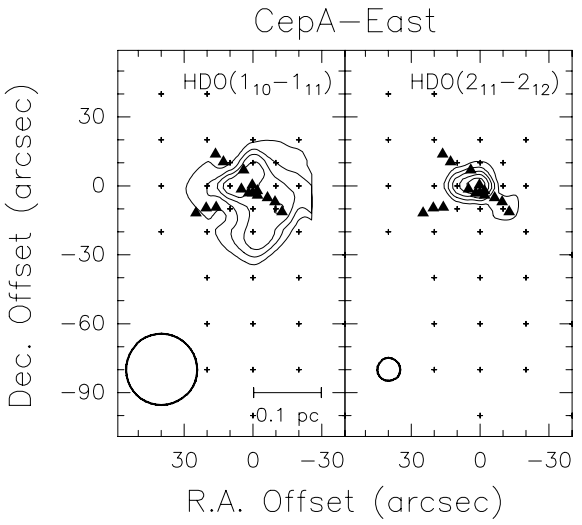

Figure 5. Contour maps of the integrated HDO $J_{\mathrm{K\_K_+}} = 1_{10}$–$1_{11}$ (upper panel) and $J_{\mathrm{K\_K_+}} = 2_{11}$–$2_{12}$ (lower panel) integrated emission towards CepA-East. Symbols are drawn as in Fig. 1. The velocity integration interval is −20, 0 km s^{-1}. The contours range from 0.14 to 0.56 K km s^{-1} (upper panel) and from 0.60 to 3.00 K km s^{-1} (lower panel). The first contours and the steps correspond to $\sim 3\sigma$.

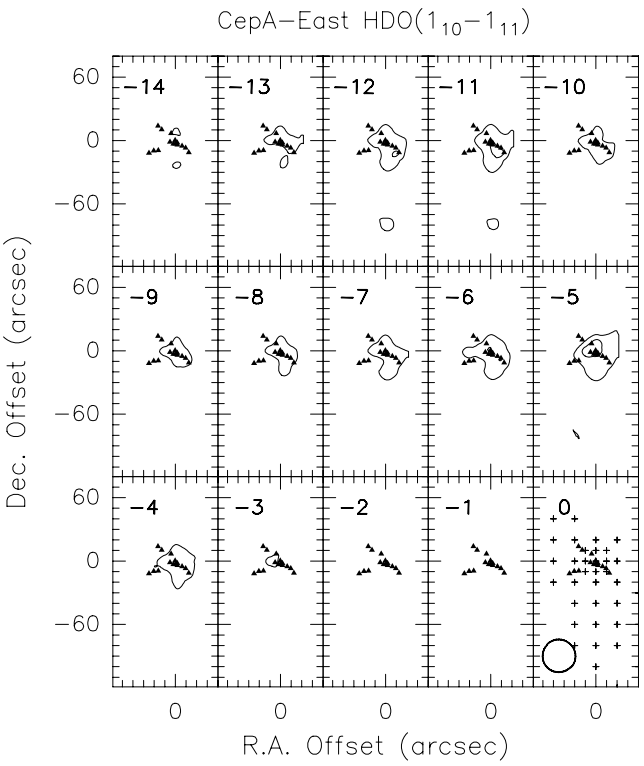

Figure 6. Channel map of the HDO $J_{\mathrm{K\_K_+}} = 1_{10}$–$1_{11}$ emission towards CepA-East. Each panel shows the emission integrated over a velocity interval of 1 km s^{-1} centred at the value given in the left-hand corner. Symbols are drawn as in Fig. 1. The ambient velocity emission is −10.7 km s^{-1} according to CS $J = 5$–4 and $C^{18}O$ $J = 2$–1 measurements (see the text). The contours range are 0.03 ($\sim 3\sigma$) and 0.06 K km s^{-1}.

indicates (i) a structure elongated along the SW direction with a peak near the centre of the map and (ii) another elongated feature pointing towards the south (see Section 3.3). On the other hand, the 2_{11}–2_{12} HDO map, obtained with higher resolution (10 arcsec), reveals a ∼15 arcsec (0.05 pc) clump centred at the HW2 coordinates, where the YSOs are located, and a second unresolved structure lying along the SW VLA jet.

In order to study the HDO kinematics, we present in Figs 6 and 7 the velocity channel maps of the 1_{10}–1_{11} and 2_{11}–2_{12} emissions, respectively. From these maps we argue that HDO in CepA-East traces the outflow activity and a small region around the driving YSOs. A quite complex scenario is therefore drawn: (i) a central component, clearly shown by the 2_{11}–2_{12} line, which is associated both with ambient velocity and higher redshifted (up to −2 km s^{-1}) velocities; (ii) a component associated with the SW VLA chain and emitting in both HDO lines; and (iii) a final component pointing towards the south and detected through the 1_{10}–1_{11} line. These last two components emit at redshifted velocities (up to −4 km s^{-1}) and at −12 and −11 km s^{-1}, i.e. at velocities close to the ambient one. Note that the −12 and −11 km s^{-1} panels of Fig. 6 seem to also indicate the possible occurrence of a HDO 1_{10}–1_{11} clump at (0, −80 arcsec), along the southern direction, suggesting a connection with the central feature pointing towards the south. This southern emission has not been detected with the 2_{11}–2_{12} line and therefore for the sake of clarity in the corresponding channel maps in Fig. 7 only a zoom of a smaller region is shown.

3.3 HDO and H_2S

In order to further investigate the southern molecular outflow, the present HDO maps can be compared with the H_2S ones reported by Codella et al. (2003). In particular, Fig. 8 shows the contour maps (thin line) of the $H_2S(1_{10}$–$1_{01})$ emission integrated over the redshifted velocity interval typical of the southern outflow: −7, −3 km s^{-1}. The HDO(1_{10}–1_{01}) map, integrated over the same velocity range, is drawn using a thick contour. From the H_2S contours it is possible to detect the SE outflow (ending at the position of clump A) and the southern outflow, which extends at the position of clump C. The HDO map is in agreement with the picture given by H_2S, both suggesting an outflow activity towards the south. This scenario could reflect different chemical and/or physical conditions for the regions where the different flows are moving. The southern outflow seems chemically enriched with respect to the typical gas composition of the dark clouds. It shows a redshifted component (see Fig. 6), whereas the blueshifted counterpart could be tentatively singled out in the emission around ∼−12 km s^{-1}, i.e. at velocities close to the ambient one, but slightly blueshifted with respect to the −10.7 km s^{-1} value. In particular, the tentative detection of HDO emission at (0, −80 arcsec) shown in the channel maps in Fig. 6 is supported by the occurrence of a H_2S red- and blueshifted (see fig. 4 of Codella et al. 2003) clump at the same position.

In Fig. 9 we summarize all the information given by the CS and HDO channel maps, drawing a schematic picture with the main clumps and outflow directions. The high-excitation HDO(2_{11}–2_{12}) line is tracing the region close to the YSOs, marked in Fig. 9 by an asterisk at (0, 0 arcsec) offset representing the HW2 coordinates. Four main flows are identified: three (SW, NE and SE) associated with the VLA sources and probably accelerating high-density material traced by CS. The SW outflow is also traced by HDO emission. In addition, HDO reveals a fourth outflow pointing towards the south and not traced by the VLA sources nor by the CS structures. Finally, we note that the highest HDO excitation conditions occur near the YSOs, where the beam deconvolved line intensity ratio $R_{\mathrm{HDO}} \simeq T_{\mathrm{mb}}(2_{11}$–$2_{12})/T_{\mathrm{mb}}(1_{10}$–$1_{01})$ is ∼2. On the other hand, the

Downloaded from https://academic.oup.com/mnras/article/361/1/244/1022325 by CNRS - ISTO user on 13 April 2021

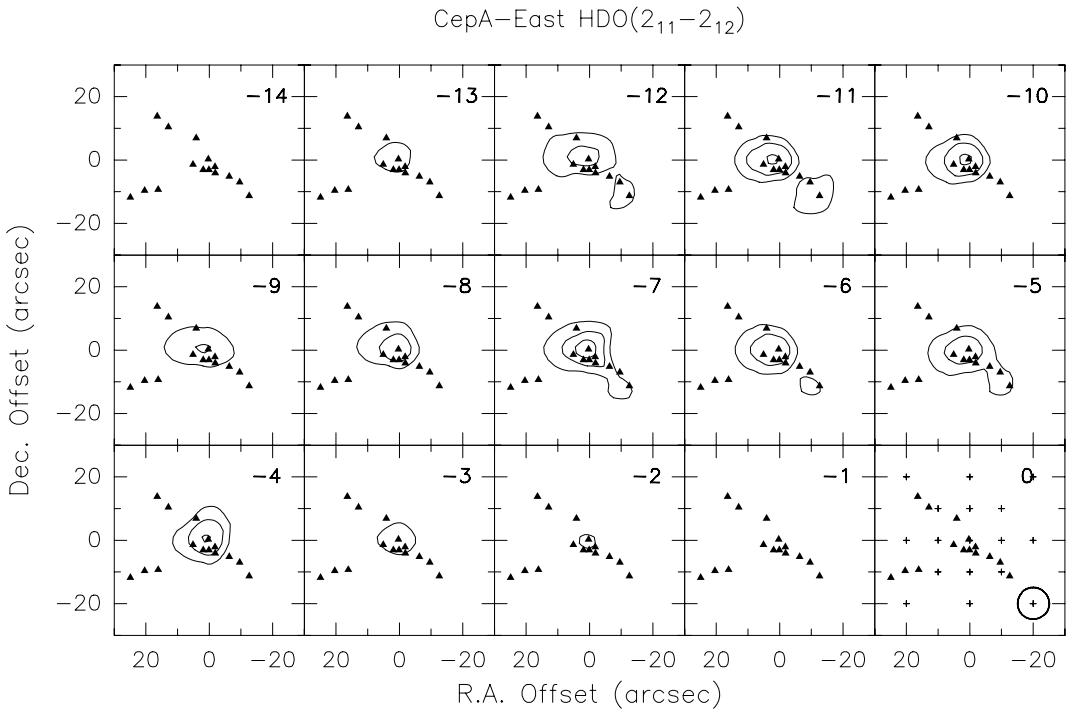

Figure 7. Zoom of the channel map of the HDO $J_{K\_K_+} = 2_{11}$–2_{12} emission towards CepA-East. Each panel shows the emission integrated over a velocity interval of 1 km s^{-1} centred at the value given in the left-hand corner. Symbols are drawn as in Fig. 1. The ambient velocity emission is −10.7 km s^{-1} according to CS $J = 5$–4 and $C^{18}O$ $J = 2$–1 measurements (see the text). The contours range are 0.12 ($\sim 3\sigma$), 0.24 and 0.36 K km s^{-1}.

southern flow suggests lower excitation conditions, with $R_{HDO} \simeq 0.6$ at the (0, −20 arcsec) offset.

4 A SPECTRAL SURVEY TOWARDS CEPA-EAST

Fig. 10 presents the most representative examples of line profiles observed towards CepA-East. Different molecules exhibit different spectral behaviours and they can be grouped into three classes, summarized in Table 3: (i) ambient species ($C^{13}CH$, C_3H_2, CH_2CO, CH_3C_2H, $HC^{18}O^+$), not detected at high velocities and with relatively narrow (3–4 km s^{-1}) lines at velocities close to the ambient one (hereafter called the ambient peak); (ii) outflow tracers (CO, CS, H_2S, SiO, SO, SO_2), which show extended wings (e.g. $v - v_{LSR}$ up to ∼30 km s^{-1} for CO and 10 km s^{-1} for SO) and span the whole range of observed velocities; and (iii) species (OCS, H_2CS, HDO and CH_3OH) which are associated with wings and, in addition, show a redshifted secondary peak at −5.5 km s^{-1} (hereafter called the outflow peak), well separated (by ∼5 km s^{-1}) from the ambient velocity. Unfortunately, the present data do not allow us to clarify the spatial distribution of the spectral outflow peak, i.e. whether it is tracing a small clump or it is related to a more extended structure. However, the comparison between HDO and H_2S emissions shown in Fig. 9 clearly suggests that the spectral outflow peak is tracing an elongated structure flowing towards the south. Only accurate CH_3OH, H_2CS and OCS maps can confirm this conclusion.

Fig. 11 displays the $CH_3OH(5_K$–$4_K)$ and $(3_K$–$2_K)$ spectra in the upper and lower panel, respectively: the dashed lines indicate the predicted positions of the hyperfine component at different excitations. Although different lines are blended, from these spectacular emissions it is possible to see that almost all the components, including those at very high excitations with $E_u \simeq 120$ K, have been detected and show the redshifted peak. It is worth noting that other very high-excitation CH_3OH lines (up to $E_u = 390$ K) have been detected serendipitously, as reported in Table 1. Finally, Fig. 12 shows the striking differences observed on the profiles of several transitions of HDO (upper panels) and H_2CS (lower panels). From these spectra, it is clear that the two HDO peaks are associated with roughly similar excitation conditions, whereas for H_2CS, the −5.5 km s^{-1} peak increases its intensity with respect to the −10.7 km s^{-1} peak with excitation indicating different physical conditions. For instance, the ratio between the mean brightness temperatures of the outflow and ambient peaks is ∼0.6 for the $J_{K\_K_+} = 7_{16}$–6_{15} transition at 60 K, while it is $\leqslant 0.1$ for the $J_{K\_K_+} = 3_{13}$–2_{12} line at 23 K.

In conclusion, the line profiles obtained indicate that at the CepA-East positions the emissions due to the clump hosting the YSOs and to the associated molecular outflows coexist and produce two distinct line peaks which suggest different excitation conditions. The results also suggest that different molecules can trace different excitation conditions at the same observed velocity. This gives us a precious opportunity to perform a multiline analysis in order to clarify the physical conditions associated with the ambient emission and those associated with the southern chemically rich molecular outflow.

5 DERIVED GAS PARAMETERS

5.1 Analysis procedures

By means of statistical-equilibrium calculations and using the four observed SO lines, it is possible to estimate the total column density (N_{tot}) as well as the kinetic temperature (T_k) and the hydrogen density (n_{H_2}). A large velocity gradient (LVG) model and the

Downloaded from https://academic.oup.com/mnras/article/361/1/244/1022325 by CNRS - ISTO user on 13 April 2021

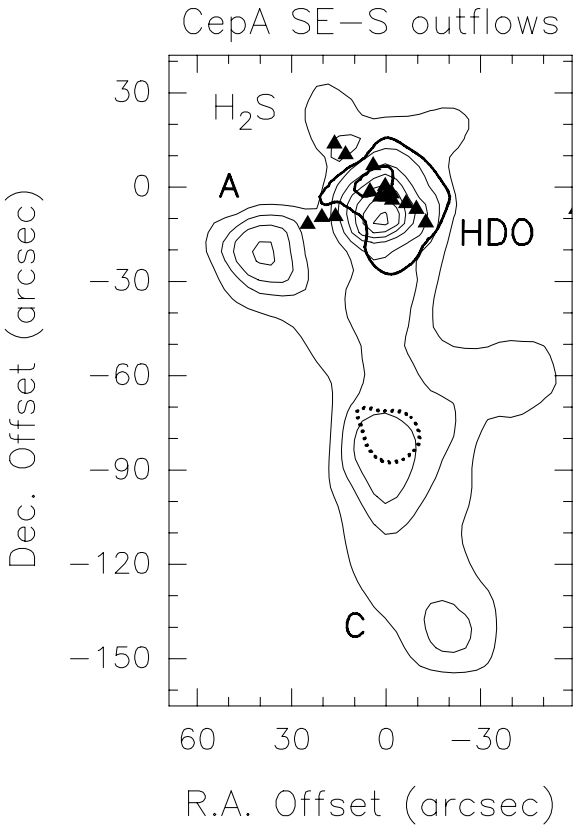

Figure 8. Contour maps (thin line) of the $H_2S(1_{10}–1_{01})$ redshifted emission (Codella et al. 2003) integrated over the velocity interval −7, −3 km s^{-1}. Two main flows are clearly drawn: one pointing to SE (and ending at clump A position), and another towards the south (ending at clump C). Symbols are drawn as in Fig. 1. The thick solid line shows the contour maps of the HDO($1_{10}–1_{01}$) emission integrated over the same range of velocity. The thick dotted line shows the distribution of the HDO($1_{10}–1_{01}$) emission integrated over the interval −13, −11 km s^{-1} and tentatively points out a blueshifted counterpart (see the channel maps of Fig. 6).

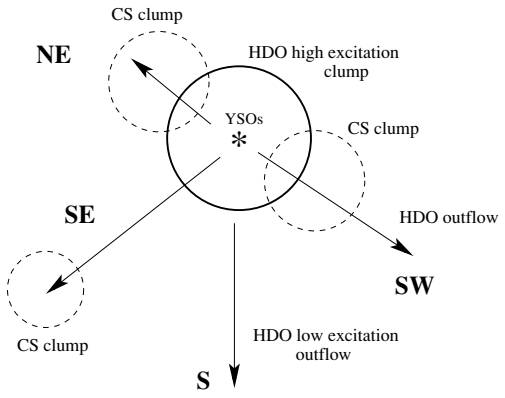

Figure 9. A schematic picture (not to scale) of the directions of the multiple outflows driven by the CepA-East YSOs as traced by HDO and CS emission (see the text). Following the channel maps four main flows are identified: three (SW, NE and SE) associated with the VLA shocked chains and with CS clumps, and one (S) traced by the HDO($1_{10}–1_{01}$) emission. The higher excitation HDO($2_{11}–2_{12}$) line well defines the SW outflow and with the central region close to the YSOs coordinates (marked by an asterisk).

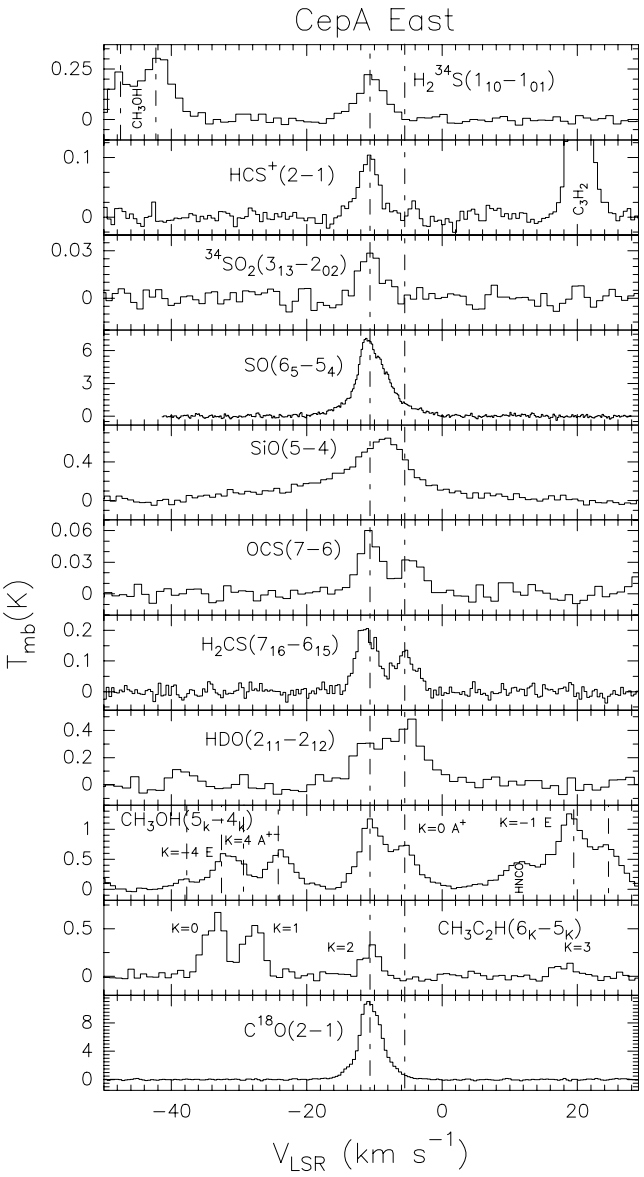

Figure 10. Molecular line profiles observed towards CepA-East: species and transitions are reported. The dashed lines denote the ambient LSR velocity (−10.65 km s^{-1}), according to the $C^{18}O$ measurement, and for the component at −5.51 km s^{-1} well outlined, for example, in the H_2CS profile. In case of the $CH_3OH(5_K–4_K)$ spectrum, four hyperfine lines at different excitations are present: $K = 0\,A^+$ ($E_u = 35$ K), $K = -1\,E$ ($E_u = 39$ K), $K = -4\,E$ ($E_u = 122$ K) and $K = 4\,A^{+-}$ ($E_u = 115$ K). The $CH_3C_2H(6_K–5_K)$ pattern shows the $K = 0$, 1, 2, 3 lines. The small vertical labels CH_3OH ($E_u = 126$ K), C_3H_2 and HNCO refers to three serendipity detections (see Table 1).

collisional rates from Green (1994) have been used. As a result of the lack of SO maps, these calculations have been performed using the mean-beam brightness temperatures relative to the intensities of the four spectra, without beam filling factor correction. If the source was definitely smaller than the four beamwidths, the LVG calculations would lead to an overestimate of the column densities (by up to a factor of 9) and of excitation conditions (by up to factors of 1.2 and 2 for T_k and n_{H_2}, respectively).

Following Cesaroni et al. (1991), statistical equilibrium computations in the LVG approximation have been used to analyse the

Downloaded from https://academic.oup.com/mnras/article/361/1/244/1022325 by CNRS - ISTO user on 13 April 2021

Table 3. Summary of the properties of the profiles observed towards CepA-East.

Molecular tracers in CepA-East		
CH_3OH, HCS^+, HDO, H_2CS, OCS	$\Longrightarrow$	Ambient, outflow and peak at -5.5 km s^{-1}
CO, CS, H_2S, SiO, SO, SO_2	$\Longrightarrow$	Ambient and outflow
$C^{13}CH$, C_3H_2, CH_2CO, CH_3C_2H, $HC^{18}O^+$	$\Longrightarrow$	Only ambient

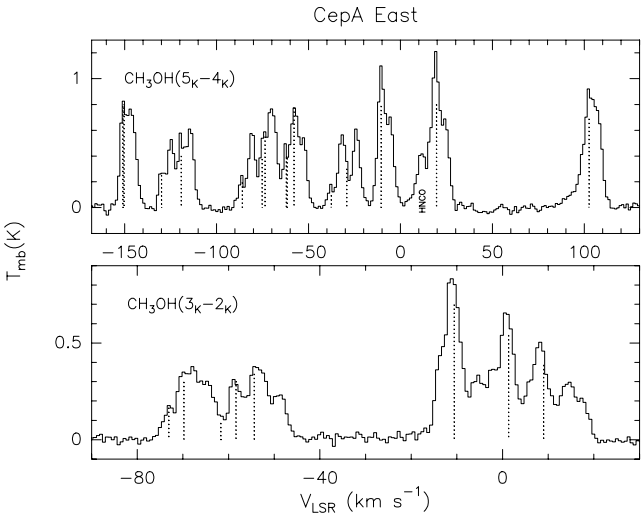

Figure 11. $CH_3OH(5_K–4_K)$ and $CH_3OH(3_K–2_K)$ line profiles observed towards CepA-East. The dotted lines denote the predicted positions of the hyperfine components at different excitations. The HNCO(11_{011}–10_{010}) line is also marked in the methanol (5_K–4_K) pattern. The velocity scale of the spectra is calculated with respect to the frequency of the 5_0–4_0A^+ (241 791.43-MHz) and 3_0–2_0A^+ (145 103.23-MHz) lines.

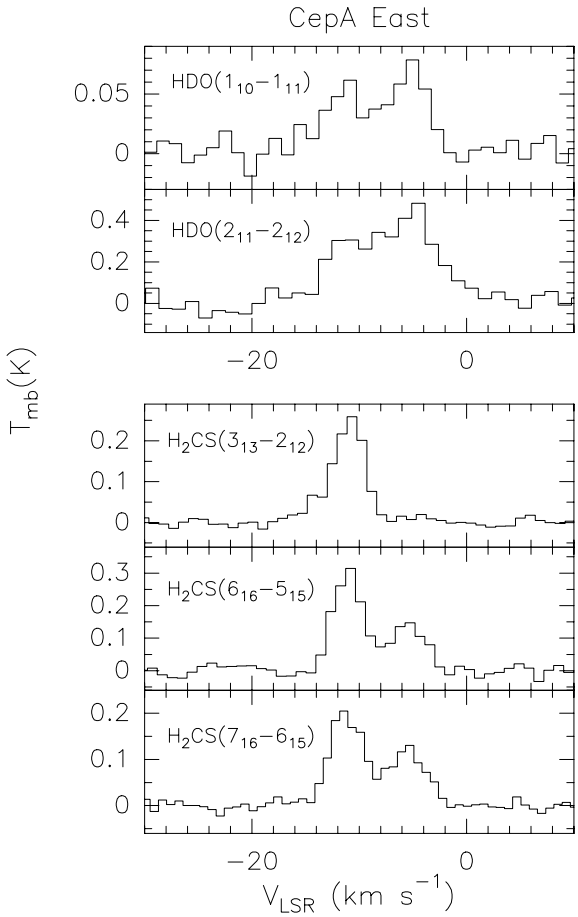

Figure 12. HDO (upper panels) and H_2CS (lower panels) line profiles observed towards CepA-East: transitions are reported (see Table 1). Note how for H_2CS the -5.5 km s^{-1} component increases its intensity with respect the -10.7 km s^{-1} peak with excitation.

CS and $C^{34}S$ spectra. In particular, for optically thin conditions, the line brightness temperatures depend only on density and, to a minor degree, on temperature. In this case, we excluded CS(2–1) which clearly shows self-absorption effects and we used CS(5–4) as well as the $C^{34}S$ lines to derive n_{H_2} estimates.

For the CH_3OH, CH_3C_2H, H_2CS and $^{34}SO_2$ molecules, observed through at least three lines, in order to estimate the rotational temperature and column densities, the standard rotation diagram method, assuming local thermaldynamic equilibrium (LTE) and optically thin conditions, has been used. For the other molecular species, the total column densities have been calculated using the constants given in the data bases for molecular spectroscopy and considering the temperature estimates derived from the LVG and rotation diagram results. For comparison, the values calculated by using the H_2S and SO_2 emissions (Codella et al. 1999) are also reported.

When possible, different column densities have been derived for the different lines at -10.7 and -5.5 km s^{-1}. In particular, the methanol patterns clearly allow us to derive different excitation conditions, while H_2CS leads to an estimate of the temperature for the -10.7 km s^{-1} component. Finally, following the SO_2 analysis of Codella et al. (2003), we have also assumed two components for CS and SO which show strong redshifted wing emission with an intense emission around -5 km s^{-1}.

5.2 Results

The derived parameters have been summarized in Table 4. The LVG results based on the SO spectra lead to kinetic temperatures of 60–100 K and $n_{H_2} \sim 5 \times 10^6$ cm^{-3} for the -10.7 km s^{-1} line at ambient velocity, while slightly higher temperatures (70–180 K) and definitely higher densities (2×10^6–6×10^7 cm^{-3}) have been derived for the -5.5 km s^{-1} component. The total SO column densities are around 4×10^{14} and 5×10^{13} cm^{-2} for the ambient and outflow components, respectively.

The CS LVG results indicate hydrogen number densities greater than 6×10^4 cm^{-3} for the ambient component. For the outflow component, the CS analysis leads to densities in the range between 4×10^3 and 5×10^4 cm^{-3}. On the other hand, the $C^{34}S$ data for the ambient component suggest lower densities with values around 2×10^4 cm^{-3}. The $C^{34}S$ emission is optically thinner than the CS one, and in fact CS shows self-absorption, whereas $C^{34}S$ shows Gaussian profiles; thus, it is reasonable to expect that $C^{34}S$ is tracing inner regions with respect to CS. In this case, the LVG results seem to give puzzling results for CepA-East with a high-density envelope and a

Downloaded from https://academic.oup.com/mnras/article/361/1/244/1022325 by CNRS - ISTO user on 13 April 2021

Table 4. Column densities, temperatures and hydrogen densities for the ambient and outflow gas components.

Molecules	Ambient				Outflow peak				
	N_{tot}[a] (cm^{-2})	T_{kin} (K)	n_{H_2} (cm^{-3})	$X[\,]/X[H_2]$[a]	N_{tot}[a] (cm^{-2})	T_{kin} (K)	n_{H_2} (cm^{-3})	$X[\,]/X[H_2]$[a]	f[b]
$C^{13}CH$	$0.6–3 \times 10^{13}$	–	–	$0.2–3 \times 10^{-8}$[c]	–	–	–	–	–
C_3H_2	$0.6–5 \times 10^{13}$	–	–	$0.2–5 \times 10^{-10}$	–	–	–	–	–
CH_2CO	$0.3–1 \times 10^{15}$	–	–	$8 \times 10^{-10}–1 \times 10^{-8}$	–	–	–	–	–
CH_3C_2H	1×10^{15}	37	–	$0.3–1 \times 10^{-8}$	–	–	–	–	–
CH_3OH	7×10^{14}	33	–	$2–7 \times 10^{-9}$	3×10^{15}	220	–	6×10^{-8}	20
CO, $C^{18}O$	$1–4 \times 10^{19}$	–	–	–	5×10^{18}	–	–	–	–
CS, $C^{34}S$	$1–5 \times 10^{14}$	–	$>6–10^4$	$0.3–5 \times 10^{-9}$	3×10^{13}	–	$4 \times 10^3–5 \times 10^4$	6×10^{-10}	1
$HC^{18}O^+$	$1–6 \times 10^{12}$	–	–	$3 \times 10^{-8}–1 \times 10^{-10}$[c]	–	–	–	–	–
HCS^+	$0.3–1 \times 10^{13}$	–	–	$8 \times 10^{-12}–1 \times 10^{-10}$	3×10^{12}	–	–	$6\ 10^{-11}$	4
HDO	$2–5 \times 10^{14}$	–	–	$0.5–5 \times 10^{-9}$	6×10^{14}	–	–	1×10^{-8}	11
H_2CS	3×10^{13}	20	–	$0.8–3 \times 10^{-10}$	1×10^{14}	–	–	2×10^{-9}	16
H_2S, $H_2{}^{34}S$[d,e]	5×10^{14}	27	–	$1–5 \times 10^{-9}$	_[d]	_[d]	_[d]	_[d]	_[d]
HNCO	$2–3 \times 10^{13}$	–	–	$0.5–3 \times 10^{-10}$	–	–	–	–	–
OCS	$2–5 \times 10^{13}$	–	–	$0.5–5 \times 10^{-10}$	5×10^{13}	–	–	$1\ 10^{-9}$	11
SiO[d]	1×10^{13}	150	2×10^6	$0.3–1 \times 10^{-10}$	_[d]	_[d]	_[d]	_[d]	_[d]
SO	4×10^{14}	60–100	$4–6 \times 10^6$	$1–4 \times 10^{-9}$	5×10^{13}	70–180	$2 \times 10^6–6 \times 10^7$	1×10^{-9}	0.7
SO_2[e]	3×10^{15}	75	–	$0.9–3 \times 10^{-8}$	1×10^{15}	130	–	$2\ 10^{-8}$	1.5
$^{34}SO_2$	1×10^{14}	200	–	$0.3–1 \times 10^{-9}$	–	–	–	–	–

[a]The column densities and the abundances regarding the species detected through only one line have been derived assuming $X[CO]/X[H_2] = 10^{-4}$ and T_{kin} = 20–100 K (ambient peak) and T_{kin} = 200 K (outflow peak), following the temperature measurements based on the CH_3C_2H, CH_3OH, SO and SO_2 emissions. [b]Average ratio between the outflow and the ambient abundances. [c]For $C^{13}CH$ and $HC^{18}O^+$, the abundances refer to the most abundant isotopomers (CCH and HCO^+) calculated assuming $^{12}C/^{13}C = 89$ and $^{16}O/^{18}O = 490$ (Wilson & Rood 1994). [d]For H_2S and SiO the ambient and outflow components cannot be disentangled; thus the values refer to the whole emission and the abundances are not reported. [e]The H_2S and SO_2 results are taken from the paper by Codella et al. (2003): the $H_2{}^{34}S$ emission has been used to derive the optical depth and consequently refine the H_2S column density.

lower-density central region. One possible solution comes from the recent results reported by Bottinelli & Williams (2004), who analyse the large-scale dynamics of CepA-East by using a density profile measured from a 850-μm map of the region. The model proposed by these authors has a high-density centre with depleted CS and an outer envelope with a low n_{H_2} and normal CS abundance. Therefore, our hydrogen density estimates could be biased by the fact that the CS abundance is varying along the central region.

The least-square fits to all detected lines in the CH_3OH rotation diagram, shown in Fig. 13, gives, for the ambient component (middle panel), rotational temperatures of ∼30 K, while the total methanol column density is $\sim 7 \times 10^{14}$ cm^{-2}. The CH_3OH temperature is confirmed by the CH_3C_2H rotation diagram which leads to 37 K. This suggests that at the ambient velocities both molecules trace similar environments. On the other hand, for the outflow component (lower panel of Fig. 13) the derived temperature is 220 K and the CH_3OH column density is 3×10^{15} cm^{-2}. However, due to the blending between ambient and outflow components for the methanol spectral patterns, the plot for the outflow component is less clear and the fit is definitely more doubtful. In any case, the comparison between the plots of the ambient component and the outflow one, which shows high-excitation (E_u = 390 K) CH_3OH emission, clearly indicates a definitely higher temperature for the outflow component.

Using the H_2CS and $^{34}SO_2$ emissions, an estimate of the rotational temperature of the ambient emission, observed in three lines, has also been obtained. The results lead to low temperatures (20 K) for H_2CS and definitely higher values (200 K) for $^{34}SO_2$, suggesting that the H_2CS spectral peak at rest velocity mainly traces relatively cool ambient material. The column densities are $N_{H_2CS} \simeq 3 \times 10^{13}$ and $N_{^{34}SO_2} \simeq 10^{14}$ cm^{-2}.

Taking into account the temperature estimates obtained from the SO and CH_3OH data, the total column densities for the molecular species observed in one or two lines have been calculated using the spectroscopic constants given in the literature and summarized in the JPL (Pickett et al. 1998), NIST (Lovas 2004), Cologne (Müller et al. 2001) and Leiden (Schöier et al. 2005) data bases and considering a kinetic temperature in the range 20–100 K for the ambient component and 200 K for the outflow one. Table 4 reports the values of the total column densities for the ambient emission: $N_{C^{13}CH}$ and $N_{C_3H_2}$ are $\sim 1 \times 10^{14}$ cm^{-2}, N_{HNCO} and $N_{OCS} \simeq 3 \times 10^{13}$ cm^{-2}, $N_{CH_2CO} \sim 5 \times 10^{15}$ cm^{-2}, $N_{HC^{18}O^+}$ and $N_{HCS^+} \sim 3–5 \times 10^{12}$ cm^{-2}, while N_{HDO} is around 3×10^{14} cm^{-2}. On the other hand, for the outflow component we have column densities around 3×10^{12}, 6×10^{14} and 5×10^{13} cm^{-2} for HCS^+, HDO and OCS, respectively. We note that the HCS^+/CS abundance ratio is quite large, ∼0.1, in the outflow peak, close to that measured in dark clouds (Ohishi, Irvine & Kaifu 1992), suggesting that the HCS^+ emission has been overestimated, due to the low signal-to-noise ratio of the HCS^+ outflow peak, and/or that the derived CS abundance is underestimated, probably due to the blending between ambient and outflow spectral components (Section 5.1).

The SiO results shown in Table 4 refer to the multiline SiO survey given by Codella, Bachiller & Reipurth (1999), whereas the H_2S and SO_2 results are taken from the paper of Codella et al. (2003): the $H_2{}^{34}S$ emission has been used here to derive the optical depth, $\tau_{(1_{10}-1_{01})} \simeq 1–2$, and consequently refine the H_2S column density. Finally, it is worth noting that for H_2S and SiO the ambient and outflow components cannot be disentangled (both show continuous extended wings), and thus the values in Table 4 refer to the whole emission.

In conclusion, we find that in CepA-East at ambient velocities (i) the gas is associated with high densities, $>10^5$ cm^{-3}, and (ii) different components at different temperatures coexist, ranging from the relatively low kinetic temperatures, less than 50 K, measured with H_2S, CH_3OH, H_2CS and CH_3C_2H, to definitely higher-temperature conditions, ∼100–200 K, obtained from the SiO, SO and SO_2

Downloaded from https://academic.oup.com/mnras/article/361/1/244/1022325 by CNRS - ISTO user on 13 April 2021

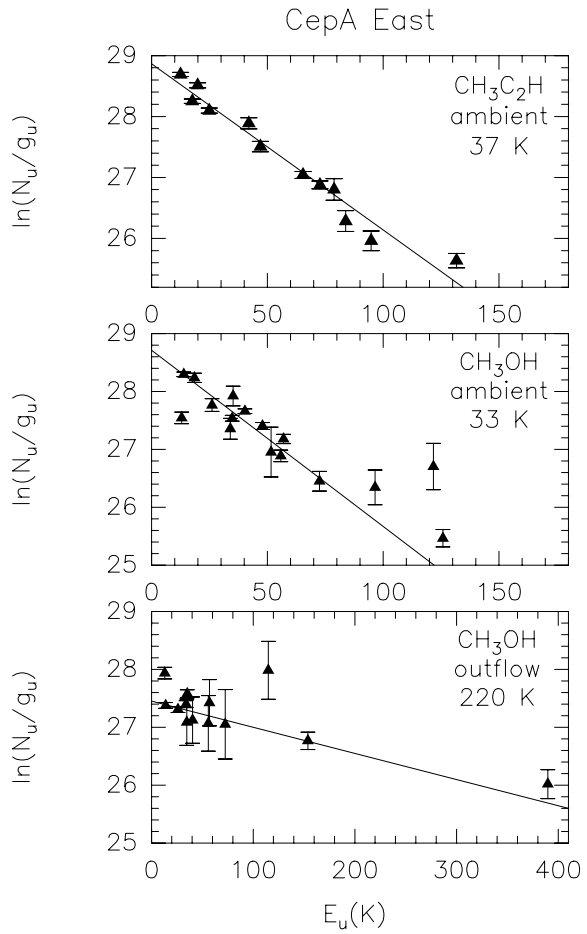

Figure 13. Rotation diagrams for the CH_3C_2H (upper panel) and CH_3OH (middle and lower panels) transitions measured towards CepA-East. For the methanol emission two spectral regimes have been considered: ambient and outflow (see the text). The parameters N_u, g_u and E_u are, respectively, the column density, the degeneracy and the energy for the upper levels of the transitions reported. The derived values of the rotational temperature are reported.

spectra. In other words, at ambient velocities we are probably sampling different layers of the high-density medium hosting the star-forming process, some of them probably being heated by the stellar radiation. On the other hand, for the outflow component we derive two density regimes: $\sim 10^4$ cm^{-3} from CS and around 10^7 cm^{-3} from SO, whereas the temperatures are always quite high: $\simeq$100–200 K, indicating regions compressed and heated by shocks.

6 DISCUSSION

6.1 Abundances

With the aim of obtaining an estimate of the abundances of the observed species, the H_2 column densities have been derived from $C^{18}O$ for the ambient component and from CO and $C^{18}O$ for the outflow peak, by assuming a standard X[CO]/X[H_2] ratio ($\simeq 10^{-4}$; Frerking, Langer & Wilson 1982; Lacy et al. 1994). We obtained the fractional abundances with respect to H_2 as the ratio between column densities and finally an enhancement factor f for each molecule has been derived as the ratio between the abundances in the outflow and in the ambient peaks. The derived values are reported in the final column of Table 4, where two classes can be distinguished. On the one hand, CS, SO and SO_2 do not show a definite abundance enhancement ($f \simeq 1$), while the HCS^+ abundance increases only by a factor of 4. On the other hand, CH_3OH, HDO, H_2CS and OCS appear to be definitely enhanced by at least one order of magnitude ($f \sim$ 10–20), confirming that these molecules are closely associated with the chemistry occurring in molecular outflows (Bachiller & Peréz Gutiérrez 1999).

Given the well-known observational difficulties of detecting the H_2O isotopomer, HDO represents (with $H_2^{18}O$) an alternative tool for investigating the occurrence of water emission in space. In fact, HDO has already been observed towards high-mass star-forming regions, mainly hot cores (e.g. Jacq et al. 1990; Helmich, van Dishoeck & Jansen 1996; Gensheimer, Mauersberger & Wilson 1996 and references therein). In addition, the high-velocity peak indicates that HDO, and thus water, is a very sensitive shock tracer in molecular outflows driven by YSOs. The present data do not allow us to give a direct estimate of the H_2O abundance. However, by assuming the cosmic [D]/[H] ratio, $\sim 1.5 \times 10^{-5}$ (Oliveira et al. 2003), or the typical [D]/[H] ratios derived for hot cores, 2–6 $\times$ 10^{-4} (Jacq et al. 1990), it is possible to roughly calculate a H_2O abundance from our HDO measurements. We therefore derive for CepA-East $X[H_2O]/X[H_2]$ in the 10^{-6}–10^{-4} range for the ambient peak and $\simeq 10^{-5}$–10^{-4} for the outflow peak, confirming that the water abundance can be extremely enhanced in star-forming regions and that H_2O is a major coolant in warm gas (van Dishoeck & Blake 1998 and references therein).

Finally, the high abundances of CH_3OH, HDO, H_2CS and OCS, which show a well-separated high-velocity range (see Figs 10 and 12), are useful tools for investigating the shocked material by comparing to those of other shock tracers such as SiO, SO and SO_2.

6.2 Different tracers at different velocities

In order to investigate the properties of the line wings which do not show the peak at -5.5 km s^{-1}, Fig. 14 reports the distribution with velocity of the brightness temperature ratio between SO(7–6) (upper panel), $SO_2(5_{24}$–$4_{13})$ (middle panel), $H_2S(1_{10}$–$1_{01})$ (lower panel) and SiO(5–4), as observed towards CepA-East. Note that for such a comparison we selected transitions observed with a similar HPBW (SO, 9 arcsec; SO_2, 10 arcsec; H_2S and SiO, 11 arcsec) and with similar excitation ($E_u \sim$ 21–35 K, see Table 1). From Fig. 14 it is possible to see the following.

(i) SiO emission dominates at the largest velocities, where the highest excitation conditions are expected. Actually, a comparison between the line profiles of different excitation transitions of H_2S and SO_2 observed towards CepA-East clearly indicates that the higher the velocity is, the higher the excitation (see fig. 8 of Codella et al. 2003).

(ii) Among the S-bearing species, SO_2 has the distribution associated with the largest width, followed by SO and finally by H_2S. This is also confirmed by the SO/H_2S, SO_2/H_2S and SO_2/SO column density ratio profiles, not shown here, which increase with velocity.

These results confirm the close association of SiO with the shocks occurring along the molecular outflows. Sputtering on dust grains is probably the most efficient mechanism that leads to a SiO abundance enhancement, although grain–grain collisions can also play a role depending on the gas density (Caselli, Hartquist & Havnes 1997; Schilke et al. 1997). However, it seems that H_2S, SO and SO_2 preferentially trace more quiescent regions than SiO. From the different widths of the resultant column density ratio profiles, we note the lack of an intense H_2S emission at the highest velocities.

Downloaded from https://academic.oup.com/mnras/article/361/1/244/1022325 by CNRS - ISTO user on 13 April 2021

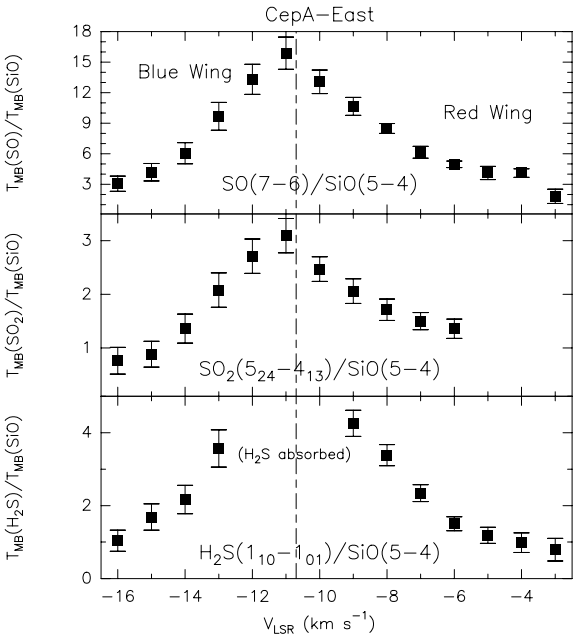

Figure 14. Distribution with velocity of the ratio between the brightness temperatures of the SO(7–6) ($E_u = 35$ K; upper panel), $H_2S(1_{10}–1_{01})$ ($E_u = 28$ K; middle panel), $SO_2(5_{24}–4_{13})$ ($E_u = 24$ K; lower panel) lines and of the SiO(5–4) ($E_u = 21$ K) profile as detected towards CepA-East. The H_2S and SO_2 data are taken from Codella et al. (2003). The HPBWs of the observations used here are: 9 arcsec (SO), 10 arcsec (SO_2) and 11 arcsec (H_2S, SiO). The dot-dashed line underlines the ambient LSR velocity according to the CS $J = 5$–4 and $C^{18}O$ $J = 2$–1 measurement.

A possible explanation is a fast conversion of H_2S into SO and SO_2 and possibly OCS, in agreement with the chemical models where first H_2S is injected from grains, then the other S-bearing species are formed very quickly over $\sim 10^3$ yr (Pineau des Forêts et al. 1993; Charnley 1997; Viti et al. 2004). Alternatively, it may be that hydrogen sulphide is not the major sulphur carrier in the grain mantles, as also suggested by the lack of H_2S features in the *ISO* spectra (Gibb et al. 2000; Boogert et al. 2000) and by the low temperature derived from the present H_2S spectra, $\sim$27 K, well in agreement with that measured by van der Tak et al. (2003, 25 K) towards high-mass star-forming regions.

On the other hand, the occurrence of the outflow peak at –5.5 km s^{-1} shows the following.

(i) OCS and H_2CS emit at high velocities, where SiO emission starts to dominate and the excitation conditions are high. At these velocities the abundance of CH_3OH, which is expected to be abundant in grain mantles and to be released in the gas phase after shocks, also definitely increases. These results suggest that OCS and H_2CS are among the sulphur carriers in the grain mantles, or that at least they are rapidly formed once the mantle is evaporated. Both scenarios are in agreement with the results by van der Tak et al. (2003) who measured high-excitation temperatures for OCS ($\sim$100 K). Unfortunately, the present data do not allow us to derive a direct temperature estimate from the OCS data. However, an estimate of the temperature of the gas traced by OCS is given by the CH_3OH emission, which well defines the OCS outflow peak and leads to a high temperature: 220 K.

(ii) HDO shows an enhancement of its fractional abundance (X[HDO]/X[H_2]) at such high velocities. From the estimated value, 10^{-8}, we can roughly infer the abundance of water assuming a D/H ratio equal to 1.5×10^{-5} (Oliveira et al. 2003): $X[H_2O]/X[H_2] \simeq 6$–10^{-4}. This suggests that the majority of oxygen here is locked into water molecules (Meyer, Jura & Cardelli 1998). This is expected if we are observing regions heated by shocks above 200 K, so that the majority of OH molecules quickly produce water through reactions with molecular hydrogen (e.g. Hartquist, Oppenheimer & Dalgarno 1980). The methanol measurements confirm the occurrence of high temperatures at these velocities.

Finally, note that sulphur could also be in atomic form when evaporated from the grain mantles, as suggested by Wakelam et al. (2004). However, the atomic S is expected to be very quickly ($\leqslant 10^3$ yr) locked into SO and SO_2, so that a large amount of atomic S is not expected to last in the gas phase for a long time and thus is difficult to observe. The form that sulphur takes on dust grains is still far from being known: the present data indicate that OCS and H_2CS may play an important role and/or that they are effectively formed in high-temperature gas.

In conclusion, the present analysis of the line profiles indicates that H_2S, SO and SO_2 may not be easily used as chemical clocks for the shocked material. On the other hand, H_2CS and OCS could be useful candidates: in the next section, a possible use of their emission is discussed.

6.3 On the origin of the outflow spectral peak

Since the outflow peak is clearly defined by two sulphuretted species such as OCS and H_2CS and by two shock tracers such as CH_3OH and HDO, we attempt to use such emission as a chemical clock. We compared the observations with the theoretical calculations recently reported by Wakelam et al. (2004). The authors developed a time-dependent chemical model of sulphur chemistry in hot cores with up-to-date reaction rate coefficients, following the molecular composition after the injection of grain mantle species into the gas phase. They found that the abundances of the main S-bearing species (H_2S, SO, OCS and SO_2) depend strongly on the physical conditions, on the oxygen abundance in the gas phase, on the adopted grain mantle composition and on the time. Hence, the use of the abundance ratios can often be useless in deriving age estimates. Nevertheless, Wakelam et al. (2004) compared the observed and predicted abundance ratios for the hot cores Orion KL and IRAS 16293−2422, for which the physical conditions had been previously obtained. The authors were able to reproduce the observed abundance and give an age estimate only assuming that a large amount of atomic sulphur is initially present in the post-evaporative gas, with $X[S]/X[H_2]$ between 3×10^{-5} and 3×10^{-6}.

In view of these results, we applied the model of Wakelam et al. (2004) to the observed emission of the CepA outflow peak. Although the model has initially been used to investigate hot cores, it follows how the S-bearing molecular abundances vary with time when the gas undergoes a sudden change in its temperature and density, and in its overall chemical abundance, because of the evaporation of grain mantles. Therefore, in principle, the model can also be reasonably used for shocked conditions occurring along a molecular outflow. However, the physical conditions and the evolution with time should be different from the hot-core case since the physical processes are different. Magneto-hydrodynamics models predict that during the passage of a shock wave, the gas temperature and density simultaneously increase before decreasing after the shock passage on timescales that depend on the model considered (e.g. Bergin, Melnik & Neufeld 1998; Flower & Pineau des Forêts 2003). In our cases,

Downloaded from https://academic.oup.com/mnras/article/361/1/244/1022325 by CNRS - ISTO user on 13 April 2021

the physical conditions are difficult to constrain in the shocked regions because we do not know how the physical conditions evolved and also because the observed molecules indicate temperature and density ranges (see Table 4). For these reasons, we considered three different models. In the first two models, the temperature and the density suddenly increase to 1000 K and 10^7 cm^{-3} and the chemistry evolves for 100 (Case 1) and 1000 yr (Case 2), respectively. After the passage of the shock, the temperature decreases to the observed values, i.e. $\simeq$200 K. The chemistry of the post-shocked gas then evolves for 10^6 yr. In the third model (Case 3), we assumed that the observed molecules mostly trace the outer material of the shock where the temperature and the density only increase to the observed values without passing through a phase with temperatures around 1000 K. This last scenario is motivated by the fact that at the CepA distance (725 pc), the filling factor relative to the shocked regions where the temperature is expected to exceed 1000 K could be definitely small and thus their emission could be strongly diluted.

From a chemical point of view, the starting point is the dark molecular cloud composition computed by the chemical model (see details of composition A in Wakelam et al. 2004). As a result of the shock passage, the molecules contained on the grain mantles, such as H_2O, H_2CO, CH_3OH and S-bearing species, are sputtered in the gas phase. For the other species, we took the abundances observed as icy features towards massive star-forming regions (see Wakelam et al. 2004).

Since the initial form and abundance of sulphur sputtered from grains is still an open question, as a first step, we decided to use the results of Wakelam et al. (2004) who reproduce reasonably well the S-bearing observations towards hot cores using a model in which sulphur is mainly evaporated from grains in atomic, OCS and H_2S forms. The initial fractional abundances are 10^{-7} for OCS and H_2S, 3×10^{-6} for the S form (Palumbo et al. 1997; van Dishoeck & Blake 1998; Wakelam et al. 2004). The implicit assumption here is that the majority of sulphur is depleted in the refractory grain cores.

Since HDO is not included in the Wakelam et al. (2004) model, we only used the abundance ratios between CH_3OH, OCS and H_2CS. Fig. 15 reports the evolution of the H_2CS/OCS (upper panels) and CH_3OH/H_2CS (lower panels) ratios as a function of time for Case 1 (shocked gas 100 yr old). The initial abundances of the three species are 9.8×10^{-8}, 8.20×10^{-11} and 3.9×10^{-6}, for OCS, H_2CS and CH_3OH, respectively. Following the physical parameters derived for the outflow peak (see Table 4) and adopting a conservative approach, we used temperatures of 100 K (left-hand panels) and 300 K (right-hand panels), whereas for the hydrogen density we assumed 10^7 cm^{-3} (dot-dashed line). The horizontal thick lines indicate the values derived from the observations towards CepA-East for the -5.5 km s^{-1} peak: 2 for H_2CS/OCS and 30 for CH_3OH/H_2CS. Fig. 15 shows that, for the assumed n_{H_2} and T_{kin} ranges, the observed ratios lead to ages for the shocked gas in the CepA-East redshifted component in the range $\sim 10^3$–3×10^4 yr. The H_2CS/OCS trend is due to a maximum of the H_2CS abundance at 10^4 yr and to a decrease of the OCS abundance after 10^3 yr. On the other hand, the CH_3OH/H_2CS trend is due to a dramatic decrease of the methanol abundance for ages $\geqslant 10^4$ yr. Note that the CH_3OH/H_2CS result solves the dichotomy given by the H_2CS/OCS ratio, which is less selective, proposing ages either $\leqslant 10^4$ yr or $\sim 10^6$ yr.

Cases 2 and 3 (shocked gas 1000 yr and warmed dark cloud) do not show significant changes and thus lead to the same conclusion, leaving open the question concerning the origin of the outflow peak: gas which passed through a hot phase or warm gas in the shock surroundings? In any case, even taking into account all the uncertainties of the column density estimates, of the abundance ratios and of the physical conditions, the comparison between the observations and the model used here allows us to obtain an age for the shocked gas in CepA-East of the order of $\sim 10^3$–3×10^4 yr. Only precise measurements of density and temperature, which are usually hampered by the high degree of confusion associated with the observed regions, can refine age estimates further. Future investigations of emission

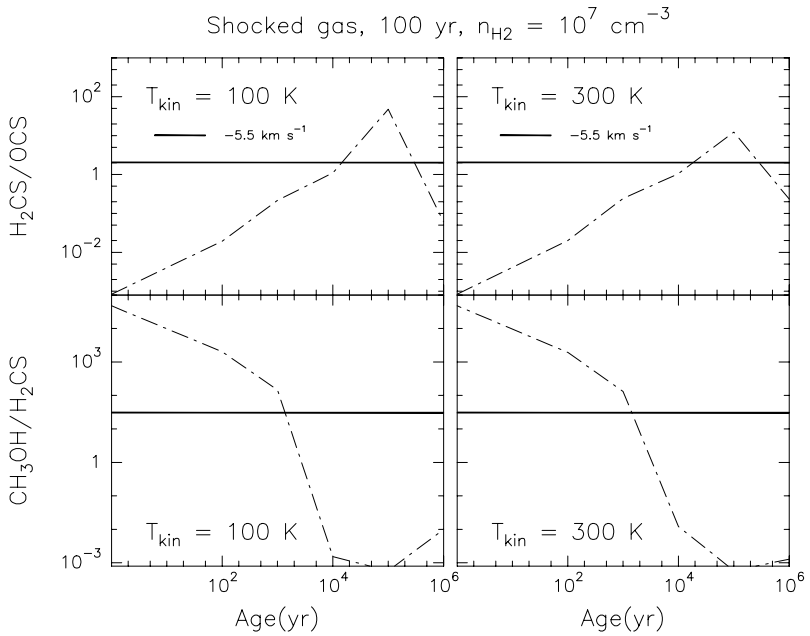

Figure 15. Evolution of the abundance ratios H_2CS/OCS (upper panels) and CH_3OH/H_2CS (lower panels) as functions of time for a gas shocked for 100 yr (see the text), a gas density of 10^7 cm^{-3}, and gas temperatures of 100 (left-hand panels) and 300 K (right-hand panels), according to the Wakelam et al. (2004) model. The horizontal thick lines indicate the values derived from the observations towards CepA-East for the -5.5 km s^{-1} peak (2 for H_2CS/OCS and 30 for CH_3OH/H_2CS, see Table 4).

Downloaded from https://academic.oup.com/mnras/article/361/1/244/1022325 by CNRS - ISTO user on 13 April 2021

due to S-bearing species towards other molecular outflows and hot cores where the physical conditions are known will confirm whether the CH_3OH/H_2CS and H_2CS/OCS abundance ratios can, in fact, be used to estimate ages.

7 SUMMARY

The CepA star-forming region has been investigated through a multiline survey at millimetre wavelengths. The results indicate the occurrence of a rich chemistry surrounding the YSOs of the CepA-East stellar association. The main findings are as follows.

(1) The CS and HDO maps draw a complex scenario, detecting high-excitation clumps hosting the YSOs driving multiple outflows. Four main flows have been identified: three are along the SW, NE and SE directions, also traced by strings of VLA continuum sources, and are accelerating high-density CS clumps. In addition, HDO reveals a fourth outflow pointing towards the south, which had been previously detected only through H_2S and SO_2 observations, and is then associated with conditions particularly favourable to a chemical enrichment.

(2) At the CepA-East position different molecules exhibit different spectral behaviours: three classes can be identified. Some species ($C^{13}CH$, C_3H_2, CH_2CO, CH_3C_2H and $HC^{18}O^+$) peak with relatively narrow lines at ambient velocities (ambient peak). Other molecules (CO, CS, H_2S, SiO, SO and SO_2) show extended wings and trace the whole range of the outflow velocities. Moreover, there is a group of species (OCS, H_2CS, HDO and CH_3OH) which shows wings and, in addition, well defines a high-velocity redshifted spectral peak (outflow peak) which can be used to investigate the SE–S outflows.

(3) The physical conditions associated with both the ambient and outflow peaks have been estimated. By means of statistical-equilibrium calculations, using LVG codes, we have obtained the physical parameters of the molecular gas traced by SO and CS. For CH_3C_2H, H_2CS, $^{34}SO_2$ and CH_3OH we have used the rotation diagram method. For the other molecular species, we have calculated the total column densities assuming LTE conditions. At ambient velocities the gas is quite dense ($>10^5$ cm^{-3}) and different components at different temperatures coexist, ranging from the relatively low kinetic temperatures ($\leqslant$50 K) measured with H_2S, CH_3OH, H_2CS and CH_3C_2H, to definitely higher-temperature conditions, $\sim$100–200 K, obtained from the SiO, SO and SO_2 spectra, which may trace layers directly heated by the stellar radiation. For the outflow component densities between $\sim10^4$ and $\sim10^7$ cm^{-3} and high temperatures, $\simeq$100–200 K, have been found, indicating regions compressed and heated by shocks.

(4) The comparison between the line profiles of different outflow tracers of molecular outflows shows that SiO dominates at the highest velocities, where the highest excitation conditions are found. This confirms the close association of SiO with shocks. On the other hand, H_2S, SO_2 and SO preferentially trace more quiescent regions. In particular, we find a lack of a bright H_2S emission at the highest velocities. Moreover, OCS and H_2CS emit at quite high velocities, where (i) SiO emission dominates and the excitation conditions are high and (ii) CH_3OH and HDO, other shock tracers, increase their abundance. These results could indicate that H_2S is not the only major sulphur carrier in the grain mantles, and that OCS and H_2CS may probably play an important role on the grains, or that alternatively they could rapidly form once the mantle is evaporated after the passage of a shock.

(5) We checked the possible use of the CH_3OH, OCS and H_2CS emission as chemical clocks to measure the age of the shocked material associated with the outflow peak. The observations have been compared with the theoretical calculations recently reported by Wakelam et al. (2004), who developed a time-dependent model with up-to-date reaction rate coefficients for the sulphur chemistry. Once associated with the derived physical parameters, the H_2CS/OCS and CH_3OH/H_2CS column density ratios led to ages in the range 10^3–3×10^4 yr. Further observations of emission due to sulphuretted molecules as well as accurate measurements of density and temperatures associated with the outflowing material are necessary in order to calibrate these chemical clocks.

ACKNOWLEDGMENTS

We are grateful to J. Santiago Garcia, M. Tafalla, C. M. Walmsley and D. A. Williams for helpful suggestions and discussions. SV acknowledges individual financial support from a PPARC Advanced Fellowship. We also thank the referee for the contribution to the improvement of the paper.

REFERENCES

Bachiller R., Peréz Gutiérrez M., 1999, ApJ, 487, L93
Bachiller R., Peréz Gutiérrez M., Kumar M. S. N., Tafalla M., 2001, A&A, 372, 899
Bergin E. A., Ungerechts H., Goldsmith P. F., Snell R. L., Irvine W. M., Schloerb F. P., 1997, ApJ, 499, 777
Bergin E. A., Melnik G. J., Neufeld D. A., 1998, ApJ, 499, 777
Boogert A. C. A., Tielens A. G. G. M., Ceccarelli C., Boonman A. M. S., van Dishoeck E. F., Keane J. V., Whittet D. C. B., de Graauw Th., 2000, A&A, 360, 683
Bottinelli S., Williams J. P., 2004, A&A, 421, 1113
Buckle J. V., Fuller G. A., 2003, A&A, 399, 567
Caselli P., Hartquist T. W., Havnes O., 1997, A&A, 322, 296
Cesaroni R., Walmsley C. M., Kömpe C., Churchwell E., 1991, A&A, 252, 278
Charnley S. B., 1997, ApJ, 481, 386
Codella C., Bachiller R., 1999, A&A, 350, 659
Codella C., Bachiller R., Reipurth B., 1999, A&A, 343, 585
Codella C., Bachiller R., Benedettini M., Caselli P., 2003, MNRAS, 341, 707
Flower D. R., Pineau des Forêts G., 2003, MNRAS, 343, 390
Frerking M. A., Langer W. D., Wilson R. W., 1982, ApJ, 262, 590
Garay G., Ramírez S., Rodríguez L. F., Curiel S., Torrelles J. M., 1996, ApJ, 459, 193
Gensheimer P. D., Mauersberger R., Wilson T. L., 1996, A&A, 314, 281
Gibb E. L. et al., 2000, ApJ, 536, 347
Goetz J. A. et al., 1998, ApJ, 504, 359
Green S., 1994, ApJ, 434, 188
Hartquist T. W., Oppenheimer M., Dalgarno A., 1980, ApJ, 236, 182
Hatchell J., Thompson M. A., Millar T. J., Macdonald G. H., 1998, A&A, 338, 713
Helmich F. P., van Dishoeck E. F., Jansen D. J., 1996, A&A, 313, 657
Jacq T., Walmsley C. M., Henkel C., Baudry A., Mauersberger R., Jewell P. R., 1990, A&A, 228, 447
Kaufman N. J., Neufeld D. A., 1996, ApJ, 456, 250
Lacy J. H., Knacke R., Geballe T. R., Tokunaga A. T., 1994, ApJ, 428, L69
Lovas F. J., 2004, J. Phys. Chem. Ref. Data, 33, 177
Meyer D. M., Jura M., Cardelli J. A., 1998, ApJ, 493, 222
Müller H. S. P., Thorwirth S., Roth D. A., Winnewisser G., 2001, A&A, 370, L49
Narayanan G., Walker C. K., 1996, ApJ, 466, 844
Ohishi M., Irvine W., Kaifu N., 1992, in Singh P. D., ed., Astrochemistry of Cosmic Phenomena. Proc. 150th Symp. of the Int. Astronomical Union,

Downloaded from https://academic.oup.com/mnras/article/361/1/244/1022325 by CNRS - ISTO user on 13 April 2021

Campos do Jordao, Sao Paulo, Brezil, August 5–9, 1991. Kluwer, Dordrecht, p. 171
Oliveira C. M., Hébrard G., Howk J. C., Kruk J. W., Chayer P., Moos H. W., 2003, ApJ, 587, 235
Palumbo M. E., Geballe T. R., Tielens A. G. G. M., 1997, ApJ, 479, 839
Pickett H. M., Poynter R. L., Cohen E. A., Delitsky M. L., Pearson J. C., Müller H. S. P., 1998, J., Quant. Spectrosc. Rad. Transfer, 60, 883
Pineau des Forêts G., Roueff E., Schilke P., Flower D. R., 1993, MNRAS, 262, 915
Sargent A. I., 1977, ApJ, 466, 844
Schilke P., Walmsley C. M., Pineau des Forêts G., Flower D. R., 1997, A&A, 321, 293
Schöier F. L., van der Tak F. F. S., van Dishoeck E. F., Black J. H., 2005, A&A, 432, 369
van der Tak F. F. S., Boonman A. M. S., Braakman R., van Dishoeck E. F., 2003, A&A, 412, 133
van Dishoeck E. F., Blake G. A., 1998, ARA&A, 36, 317
Viti S., Collings M. P., Dever J. W., McCoustra M. R. S., Williams D. A., 2004, MNRAS, 354, 1141
Wakelam V., Caselli P., Herbst E., Ceccarelli C., Castets A., 2004, A&A, 422, 159
Wilson T. L., Rood R. T., 1994, ARA&A, 32, 191

This paper has been typeset from a TEX/LATEX file prepared by the author.

Downloaded from https://academic.oup.com/mnras/article/361/1/244/1022325 by CNRS - ISTO user on 13 April 2021